

Near-ML Signal Detection in Large-Dimension Linear Vector Channels Using Reactive Tabu Search

N. Srinidhi, Saif K. Mohammed, A. Chockalingam, and B. Sundar Rajan

Abstract—Low-complexity near-optimal signal detection in large dimensional communication systems is a challenge. In this paper, we present a reactive tabu search (RTS) algorithm, a heuristic based combinatorial optimization technique, to achieve low-complexity near-maximum likelihood (ML) signal detection in linear vector channels with large dimensions. Two practically important large-dimension linear vector channels are considered: *i*) multiple-input multiple-output (MIMO) channels with large number (tens) of transmit and receive antennas, and *ii*) severely delay-spread MIMO inter-symbol interference (ISI) channels with large number (tens to hundreds) of multipath components. These channels are of interest because the former offers the benefit of increased spectral efficiency (several tens of bps/Hz) and the latter offers the benefit of high time-diversity orders. Our simulation results show that, while algorithms including variants of sphere decoding do not scale well for large dimensions, the proposed RTS algorithm scales well for signal detection in large dimensions while achieving increasingly closer to ML performance for increasing number of dimensions.

Index Terms—Linear vector channels, large dimensions, low-complexity detection, near-ML performance, V-BLAST, non-orthogonal STBCs, MIMO-ISI channels, UWB, severe delay spread, tabu search.

I. INTRODUCTION

Large-dimension communication systems are likely to play an important role in modern wireless communications, where dimensions can be in space, time, frequency and their combinations. Large dimensions can bring several advantages with respect to the performance of communication systems. For example, use of large number of transmit/receive antennas increases the number of spatial dimensions, which results in increased capacity [1],[2]. A severely delay-spread inter-symbol interference (ISI) channel (i.e., large number of echoes of the transmitted signal in time dimension), as witnessed in ultrawideband (UWB) systems, can provide the opportunity for increased time-diversity [3]. Harnessing such benefits of large-dimensions in practice, however, is challenging. In particular, optimum receiver complexity can become practically infeasible in large dimensions. Consequently, low-complexity receiver techniques/algorithms that scale well for large dimensions while achieving near-optimal performance are of interest. It has been found that many modern meta-heuristic algorithms give near-optimal performance at a much reduced complexity [4]. In this paper, we report one such heuristic based on *tabu search* [5],[6], and illustrate its near-optimal performance in two practically important large dimension systems, namely *i*)

a ‘large-MIMO system’ with *tens of transmit/receive antennas* (with a motivation to achieve high spectral efficiencies), and *ii*) a severely delay-spread MIMO UWB system with *tens to hundreds of multipath components* (with a motivation to achieve high time-diversity orders).

Tabu search (TS) is a heuristic originally designed to obtain approximate solutions to combinatorial optimization problems [5]-[8]. TS is increasingly being applied in communication problems [9]-[11]. For e.g., in [9], design of constellation label maps to maximize asymptotic coding gain is formulated as a quadratic assignment problem, which is solved using a reactive TS (RTS) strategy [8]. RTS approach is shown to be effective in terms of bit error performance and efficient in terms of computational complexity in CDMA multiuser detection [10]. In [11], a *fixed* TS based detection in V-BLAST is presented for small number of antennas. A key objective in this paper is to propose a *reactive* tabu search based approach to seek approximately maximum-likelihood (ML) solutions in large dimension problems (but with significantly lower computational complexity than that of the true ML solution) in linear vector channels (LVC) in general, and to establish its performance and complexity in two interesting communication systems in particular.

The first communication system we consider is a large-MIMO system that employs tens of transmit antennas to achieve high spectral efficiencies – e.g., a 16×16 V-BLAST system with 16-QAM and rate-3/4 turbo code can achieve a spectral efficiency of 48 bps/Hz. We show that the RTS algorithm achieves increasingly closer to ML performance for increasing number of transmit antennas (we refer to this behavior of the algorithm as the ‘large-dimension behavior’). For e.g., in a 64×64 V-BLAST system with 4-QAM, RTS is shown to achieve 10^{-3} uncoded BER at an SNR of just 0.4 dB away from single-input single-output (SISO) AWGN performance. We present a comparison of the performance and complexity of RTS with those of low-complexity variants of sphere decoders (SD), including a suboptimal fixed-complexity SD (FSD) reported in [12]. In a 32×32 V-BLAST system with 4-QAM, RTS is shown to perform better than FSD by about 1.5 dB at 10^{-2} uncoded BER. Interestingly, RTS achieves this better performance at about an order less complexity than FSD. We also show that RTS can achieve near-ML performance in decoding large non-orthogonal space-time codes (STBCs) from cyclic division algebras (CDA), which can offer full transmit diversity in addition to achieving full rate as in V-BLAST [14],[15].

The second communication scenario considered is equalization in severely delay-spread MIMO-ISI UWB channels

This work in part was presented in IEEE ISIT’2009, Seoul, Korea, July 2009, and is accepted for presentation in IEEE GLOBECOM’2009, Honolulu, USA, December 2009.

The authors are with the Department of Electrical Communication Engineering, Indian Institute of Science, Bangalore-560012, India.

with large number of multipath components (MPC). Communication systems using UWB techniques typically have very high transmission bandwidths to accommodate very high data rates [3]. Such UWB channels are characterized by severe ISI due to large delay spreads [17]-[20]. The number of MPCs in indoor and industrial environments has been observed to be of the order of several tens to hundreds; number of MPCs ranging from 12 to 120 are common in UWB channel models [17],[20]. These MPCs, if carefully exploited, can provide the opportunity to achieve increased time-diversity benefits [17]. Algorithms based on likelihood ascent search (LAS)/bit flipping [22],[23],[28] and factor graphs [27] have been proposed for equalization in such systems. We show that the proposed RTS algorithm achieves increasingly close to optimal performance for increasing number of MPCs, and achieves better performance due its inherent escape strategy from local minima.

The rest of the paper is organized as follows. The proposed RTS algorithm for detection in linear vector channels is presented in Section II. BER performance and complexity of the RTS algorithm in comparison with those of other detectors including variants of sphere decoders are presented in Sections III to V. Conclusions are presented in Sections VI.

II. PROPOSED RTS BASED DETECTION IN LVCs

We consider linear vector channels where a d_t -dimensional input vector¹ $\mathbf{x} \in \mathbb{A}^{d_t}$ (\mathbb{A} denotes a finite set from the complex field) is linearly transformed by a $d_r \times d_t$ channel transfer matrix, $\mathbf{H} \in \mathbb{C}^{d_r \times d_t}$, and is corrupted by a d_r -dimensional noise vector, $\mathbf{n} \in \mathbb{C}^{d_r}$, so that the d_r -dimensional output vector, $\mathbf{y} \in \mathbb{C}^{d_r}$, is given by

$$\mathbf{y} = \mathbf{H}\mathbf{x} + \mathbf{n}. \quad (1)$$

In communication systems, \mathbf{x} and \mathbf{y} can be the transmitted and received signal vectors, respectively, and the goal is to obtain an estimate of the transmitted vector \mathbf{x} , given \mathbf{y} and the knowledge of \mathbf{H} . When the noise is Gaussian, the maximum-likelihood (ML) detection rule is given by

$$\hat{\mathbf{x}}_{ML} = \arg \min_{\mathbf{x} \in \mathbb{A}^{d_t}} \|\mathbf{y} - \mathbf{H}\mathbf{x}\|^2 = \arg \min_{\mathbf{x} \in \mathbb{A}^{d_t}} \phi(\mathbf{x}), \quad (2)$$

where $\phi(\mathbf{x}) \triangleq \mathbf{x}^H \mathbf{H}^H \mathbf{H} \mathbf{x} - 2\Re(\mathbf{y}^H \mathbf{H} \mathbf{x})$. The computational complexity in (2) is exponential in d_t , which is prohibitive for large d_t . Our interest is to achieve near-ML performance for large d_t at low complexities. In the following subsection, we present a RTS based detection algorithm which is a low-complexity iterative local search algorithm suited well for large d_t .

A. RTS Algorithm

The RTS algorithm starts with an initial solution vector, defines a neighborhood around it (i.e., defines a set of neigh-

boring vectors based on a neighborhood criteria), and moves to the best vector among the neighboring vectors (even if the best neighboring vector is worse, in terms of likelihood, than the current solution vector; this allows the algorithm to escape from local minima). This process is continued for a certain number of iterations, after which the algorithm is terminated and the best among the solution vectors in all the iterations is declared as the final solution vector. In defining the neighborhood of the solution vector in a given iteration, the algorithm attempts to avoid cycling by making the moves to solution vectors of the past few iterations as ‘tabu’ (i.e., prohibits these moves), which ensures efficient search of the solution space. The number of these past iterations is parametrized as the ‘tabu period.’ The search is referred to as fixed tabu search if the tabu period is kept constant. If the tabu period is dynamically changed (e.g., increase the tabu period if more repetitions of the solution vectors are observed in the search path), then the search is called reactive tabu search. We consider reactive tabu search in this paper because of its robustness (choice of a good fixed tabu period can be tedious).

Neighborhood Definition: Let M denote the cardinality of $\mathbb{A} = \{a_1, a_2, \dots, a_M\}$. Define a set $\mathcal{N}(a_q)$, $q \in \{1, \dots, M\}$, as a fixed subset of $\mathbb{A} \setminus a_q$, which we refer to as the *symbol-neighborhood* of a_q . We choose the cardinality of this set to be the same for all a_q , $q = 1, \dots, M$; i.e., we take $|\mathcal{N}(a_q)| = N$, $\forall q$. Note that the maximum and minimum values of N are $M - 1$ and 1, respectively. We choose the symbol neighborhood based on Euclidean distance, i.e., for a given symbol, those N symbols which are the nearest will form its neighborhood; the nearest symbol will be the first neighbor, the next nearest symbol will be the second neighbor, and so on. For e.g., $\mathbb{A} = \{-3, -1, 1, 3\}$ for 4-PAM, and choosing N to be 2, $\mathcal{N}(-3) = \{-1, 1\}$, $\mathcal{N}(-1) = \{-3, 1\}$, $\mathcal{N}(1) = \{-1, 3\}$, $\mathcal{N}(3) = \{1, -1\}$ are possible symbol-neighborhoods. Let $w_v(a_q)$, $v = 1, \dots, N$ denote the v th element in $\mathcal{N}(a_q)$; i.e., we say $w_v(a_q)$ is the v th symbol-neighbor of a_q .

Let $\mathbf{x}^{(m)} = [x_1^{(m)} x_2^{(m)} \dots x_{d_t}^{(m)}]$ denote the data vector belonging to the solution space in the m th iteration, where $x_i^{(m)} \in \mathbb{A}$. We refer to the vector

$$\mathbf{z}^{(m)}(u, v) = [z_1^{(m)}(u, v) z_2^{(m)}(u, v) \dots z_{d_t}^{(m)}(u, v)] \quad (3)$$

as the (u, v) th *vector-neighbor* (or simply the (u, v) th neighbor) of $\mathbf{x}^{(m)}$, $u = 1, \dots, d_t$, $v = 1, \dots, N$, if *i)* $\mathbf{x}^{(m)}$ differs from $\mathbf{z}^{(m)}(u, v)$ in the u th coordinate only, and *ii)* the u th element of $\mathbf{z}^{(m)}(u, v)$ is the v th symbol-neighbor of $x_u^{(m)}$. That is,

$$z_i^{(m)}(u, v) = \begin{cases} x_i^{(m)} & \text{for } i \neq u \\ w_v(x_u^{(m)}) & \text{for } i = u. \end{cases} \quad (4)$$

So we will have $d_t N$ vectors which differ from a given vector in the solution space in only one coordinate. These $d_t N$ vectors form the neighborhood of the given vector. We note that neighborhood definition based on *bit-flipping* [21],[22] is a special case of the above neighborhood definition for $M = 2$, $N = 1$. An operation on $\mathbf{x}^{(m)}$ which gives $\mathbf{x}^{(m+1)}$

¹Notation: Vectors and matrices are denoted by boldface lowercase letters and boldface uppercase letters, respectively. $(\cdot)^*$, $[\cdot]^T$, and $[\cdot]^H$ denote conjugation, transpose and Hermitian operations, respectively. $|\cdot|$ denotes the absolute value operator. $\mathbf{A}(i, j)$ denotes the element in the i th row and j th column of matrix \mathbf{A} . a_i denotes the i th element of the vector \mathbf{a} . $\Re(\cdot)$ and $\Im(\cdot)$ denote the real and imaginary parts of a complex argument, and $j = \sqrt{-1}$. \mathbf{I}_n denotes the $n \times n$ identity matrix.

belonging to the vector-neighborhood of $\mathbf{x}^{(m)}$ is called a *move*. The algorithm is said to execute a move (u, v) if $\mathbf{x}^{(m+1)} = \mathbf{z}^{(m)}(u, v)$. We note that the number of candidates to be considered for a move in any one iteration is $d_t N$. Also, the overall number of ‘distinct’ moves possible is $d_t M N$, which is the cardinality of the union of all moves from all M^{d_t} possible solution vectors. The tabu value of a move, which is a non-negative integer, means that the move cannot be considered for that many number of subsequent iterations, unless certain conditions are satisfied.

Tabu Matrix: A *tabu_matrix* \mathbf{T} of size $d_t M \times N$ is the matrix whose entries denote the tabu values of moves. For each coordinate of the solution vector (there are d_t coordinates), there are M rows in \mathbf{T} , where each row corresponds to one symbol in the modulation alphabet \mathbb{A} ; the indices of the rows for the u th coordinate are from $(u-1)M+1$ to uM , $u \in \{1, \dots, d_t\}$. The N columns of \mathbf{T} correspond to the N symbol-neighbors of the symbol corresponding to each row. In other words, the (r, s) th entry of the *tabu_matrix*, $r = 1, \dots, d_t M$, $s = 1, \dots, N$, corresponds to the move (u, v) from $\mathbf{x}^{(m)}$ when $u = \lfloor \frac{r-1}{M} \rfloor + 1$, $v = s$ and $x_u^{(m)} = a_q$, where $q = \text{mod}(r-1, M) + 1$. The entries of the tabu matrix, which are non-negative integers, are updated in each iteration, and they are used to decide the direction in which the search proceeds (as described in the algorithm description below).

Algorithm: Let $\mathbf{g}^{(m)}$ be the vector which has the least ML cost found till the m th iteration of the algorithm. Let l_{rep} be the average length (in number of iterations) between two successive occurrences of a solution vector (repetitions). Tabu period, P , a dynamic non-negative integer parameter, is defined as follows: if a move is marked as tabu in an iteration, it will remain as tabu for P subsequent iterations unless the move results in a better solution. A binary flag, $lflag \in \{0, 1\}$, is used to indicate whether the algorithm has reached a local minima in a given iteration or not; this flag is used in the evaluation of the stopping criterion of the algorithm. The algorithm starts with an initial solution vector $\mathbf{x}^{(0)}$, which, for e.g., could be the MMSE or matched filter output vector. Set $\mathbf{g}^{(0)} = \mathbf{x}^{(0)}$, $l_{rep} = 0$, and $P = P_0$. All the entries of the *tabu_matrix* are set to zero. Define $\mathbf{y}_{MF} \triangleq \mathbf{H}^H \mathbf{y}$, and $\mathbf{R} \triangleq \mathbf{H}^H \mathbf{H}$. Compute \mathbf{y}_{MF} and \mathbf{R} . The following steps 1) to 3) are performed in each iteration. Consider m th iteration in the algorithm, $m \geq 0$.

Step 1): Initialize $lflag = 0$. Define $\mathbf{f}^{(m)} \triangleq \mathbf{R}\mathbf{x}^{(m)} - \mathbf{y}_{MF}$. Let $\mathbf{e} = \mathbf{z}^{(m)}(u, v) - \mathbf{x}^{(m)}$. The ML costs of the $d_t N$ neighbors of $\mathbf{x}^{(m)}$, namely, $\mathbf{z}^{(m)}(u, v)$, $u = 1, \dots, d_t$, $v = 1, \dots, N$, are computed as

$$\begin{aligned} \phi(\mathbf{z}^{(m)}(u, v)) &= (\mathbf{x}^{(m)} + \mathbf{e})^H \mathbf{R} (\mathbf{x}^{(m)} + \mathbf{e}) - 2\Re\left((\mathbf{x}^{(m)} + \mathbf{e})^H \mathbf{y}_{MF}\right) \\ &= \phi(\mathbf{x}^{(m)}) + 2\Re\left(\mathbf{e}^H \mathbf{R} \mathbf{x}^{(m)}\right) + \mathbf{e}^H \mathbf{R} \mathbf{e} - 2\Re\left(\mathbf{e}^H \mathbf{y}_{MF}\right) \\ &= \phi(\mathbf{x}^{(m)}) + 2\Re\left(\mathbf{e}^H \left(\mathbf{R} \mathbf{x}^{(m)} - \mathbf{y}_{MF}\right)\right) + \mathbf{e}^H \mathbf{R} \mathbf{e} \\ &= \phi(\mathbf{x}^{(m)}) + 2\Re\left(\mathbf{e}^H \mathbf{f}^{(m)}\right) + \mathbf{e}^H \mathbf{R} \mathbf{e} \\ &= \phi(\mathbf{x}^{(m)}) + 2\Re\left(\underbrace{\mathbf{e}_u^* f_u^{(m)}}_{\triangleq C(u, v)}\right) + |e_u|^2 \mathbf{R}(u, u), \end{aligned} \quad (5)$$

where the last step follows since only one coordinate of \mathbf{e} is non-zero, and $\mathbf{R}(u, u)$ is the (u, u) th element of \mathbf{R} . $\phi(\mathbf{x}^{(m)})$ on the RHS in (5) can be dropped since it will not affect the cost minimization. Let

$$(u_1, v_1) = \arg \min_{u, v} C(u, v). \quad (6)$$

The move (u_1, v_1) is accepted if any one of the following two conditions is satisfied:

$$\phi(\mathbf{z}^{(m)}(u_1, v_1)) < \phi(\mathbf{g}^{(m)}) \quad (7)$$

$$\mathbf{T}((u_1 - 1)M + q, v_1) = 0, \quad (8)$$

where q is such that $a_q = x_{u_1}^{(m)}$, $a_q \in \mathbb{A}$. If move (u_1, v_1) is not accepted (i.e., neither of the conditions in (7) and (8) is satisfied), find (u_2, v_2) such that

$$(u_2, v_2) = \arg \min_{u, v: u \neq u_1, v \neq v_1} C(u, v), \quad (9)$$

and check for acceptance of the (u_2, v_2) move. If this also cannot be accepted, repeat the procedure for (u_3, v_3) , and so on. If all the $d_t N$ moves are tabu, then all the *tabu_matrix* entries are decremented by the minimum value in the *tabu_matrix*; this goes on till one of the moves becomes acceptable. Let (u', v') be the index of the neighbor with the minimum cost for which the move is permitted. Make

$$\mathbf{x}^{(m+1)} = \mathbf{z}^{(m)}(u', v'). \quad (10)$$

The variables q', q'', v'' are implicitly defined by $a_{q'} = x_{u'}^{(m)} = w_{v''}(x_{u'}^{(m+1)})$, and $a_{q''} = x_{u'}^{(m+1)}$, where $a_{q'}, a_{q''} \in \mathbb{A}$. It is noted that in this *Step 1* of the algorithm, essentially the best permissible vector-neighbor is chosen as the solution vector for the next iteration.

Step 2): The new solution vector obtained from *Step 1* is checked for repetition. For the linear vector channel model in (1), repetition can be checked by comparing the ML costs of the solutions in the previous iterations. If there is a repetition, the length of the repetition from the previous occurrence is found, the average length, l_{rep} , is updated, and the tabu period P is modified as $P = P + 1$. If the number of iterations elapsed since the last change of the value of P exceeds βl_{rep} , for a fixed $\beta > 0$, make $P = \max(1, P - 1)$. After a move (u', v') is accepted, if $\phi(\mathbf{x}^{(m+1)}) < \phi(\mathbf{g}^{(m)})$, make

$$\mathbf{T}((u' - 1)M + q', v') = \mathbf{T}((u' - 1)M + q'', v'') = 0, \quad (11)$$

$$\mathbf{g}^{(m+1)} = \mathbf{x}^{(m+1)}, \quad (12)$$

else

$$\mathbf{T}((u' - 1)M + q', v') = \mathbf{T}((u' - 1)M + q'', v'') = P + 1, \quad (13)$$

$$lflag = 1, \quad \mathbf{g}^{(m+1)} = \mathbf{g}^{(m)}. \quad (14)$$

It is noted that this *Step 2* of the algorithm implements the ‘reactive’ part in the search, by dynamically changing P .

Step 3): Update the entries of the *tabu_matrix* as

$$\mathbf{T}(r, s) = \max\{\mathbf{T}(r, s) - 1, 0\}, \quad (15)$$

for $r = 1, \dots, d_t M$, $s = 1, \dots, N$, and update $\mathbf{f}^{(m)}$ as

$$\mathbf{f}^{(m+1)} = \mathbf{f}^{(m)} + \left(z_{u'}^{(m)}(u', v') - x_{u'}^{(m)} \right) \mathbf{R}_{u'}, \quad (16)$$

where $\mathbf{R}_{u'}$ is the u' 'th column of \mathbf{R} . The algorithm terminates in *Step 3* if the following stopping criterion is satisfied, else it goes back to *Step 1*.

Stopping criterion: The algorithm can be stopped based on a fixed number of iterations. Though convergence can be slow at low SNRs, it can be fast at moderate to high SNRs. So rather than fixing a large number of iterations to stop the algorithm irrespective of the SNR, we use an efficient stopping criterion which makes use of the knowledge of the best ML cost found till the current iteration, as follows. Since the ML criterion is to minimize $\|\mathbf{H}\mathbf{x} - \mathbf{y}\|^2$, the minimum value of the objective function $\phi(\mathbf{x})$ is always greater than $-\mathbf{y}^H \mathbf{y}$. We stop the algorithm when the least ML cost achieved in an iteration is within certain range of the global minimum, which is $-\mathbf{y}^H \mathbf{y}$. We stop the algorithm in the m 'th iteration, only if $lflag = 1$ and the condition

$$\frac{|\phi(\mathbf{g}^{(m)}) - (-\mathbf{y}^H \mathbf{y})|}{|-\mathbf{y}^H \mathbf{y}|} < \alpha_1 \quad (17)$$

is met with at least min_iter iterations being completed to make sure the search algorithm has 'settled.' The bound is gradually relaxed as the number of iterations increase and the algorithm is terminated when

$$\frac{|\phi(\mathbf{g}^{(m)}) - (-\mathbf{y}^H \mathbf{y})|}{|-\mathbf{y}^H \mathbf{y}|} < m\alpha_2. \quad (18)$$

In (17) and (18), α_1 and α_2 are positive constants. In addition, we terminate the algorithm whenever the number of repetitions of solutions exceeds max_rep . Also, the maximum number of iterations is set to max_iter .

B. RTS algorithm versus LAS algorithm

It is noted that the likelihood ascent search (LAS) algorithm presented in [21]-[23] is also a local neighborhood search based algorithm, where the basic definition of neighborhood is the same as in RTS. However, LAS differs from RTS in the following aspects: *i*) while the definition of neighborhood is static in LAS for all iterations, in RTS, in addition to the basic neighborhood definition, there is also a dynamic aspect to the neighborhood definition by way of prohibiting certain vectors from being included in the neighbor list (implemented through repetition checks/tabu period), and *ii*) while LAS gets trapped in the local minima that it first encounters and declares this minima to be the final solution vector, RTS can potentially find better minimas because of the escape strategy embedded in the algorithm (by way of allowing to pick and move to the best neighbor even if that neighbor has a lesser likelihood than the current solution vector).

It is further noted that a general version of LAS reported in [23], termed as multistage LAS (MLAS), executes a different escape mechanism when it encounters a local minima, by changing the neighborhood definition: it considers vectors which differ in two or more coordinates (as opposed to

only one coordinate in the basic neighborhood definition) as neighbors. On escaping from a local minima, the algorithm reverts back to the basic neighborhood definition till the next local minima is encountered and stops when no escape from a local minima is possible. Since the performance gain of MLAS compared to LAS is found to be small, we limit our comparison of RTS with only LAS. Our simulation results for the systems considered in Sections III to V show that RTS performs better than LAS.

III. RTS PERFORMANCE IN LARGE V-BLAST SYSTEMS

Consider a V-BLAST MIMO system with N_t transmit and N_r receive antennas. For this system, in the received signal model in (1), $\mathbf{x} \in \mathbb{A}^{N_t}$ is the transmitted symbol vector, where \mathbb{A} is the modulation alphabet, $\mathbf{H} \in \mathbb{C}^{N_r \times N_t}$ is the channel gain matrix whose entries are modeled as $\mathcal{CN}(0, 1)$, $\mathbf{y} \in \mathbb{C}^{N_r}$ is the received signal vector, and $\mathbf{n} \in \mathbb{C}^{N_r}$ is the noise vector whose entries are modeled as i.i.d $\mathcal{CN}(0, \sigma^2 = \frac{N_t E_s}{\gamma})$, where E_s is the average energy of the transmitted symbols and γ is the average received SNR per receive antenna. We rewrite the complex system model in (1) as a real-valued system as

$$\tilde{\mathbf{y}} = \tilde{\mathbf{H}} \tilde{\mathbf{x}} + \tilde{\mathbf{n}}, \quad (19)$$

where

$$\tilde{\mathbf{H}} = \begin{bmatrix} \Re(\mathbf{H}) & -\Im(\mathbf{H}) \\ \Im(\mathbf{H}) & \Re(\mathbf{H}) \end{bmatrix}, \quad \tilde{\mathbf{y}} = \begin{bmatrix} \Re(\mathbf{y}) \\ \Im(\mathbf{y}) \end{bmatrix}, \\ \tilde{\mathbf{x}} = \begin{bmatrix} \Re(\mathbf{x}) \\ \Im(\mathbf{x}) \end{bmatrix}, \quad \tilde{\mathbf{n}} = \begin{bmatrix} \Re(\mathbf{n}) \\ \Im(\mathbf{n}) \end{bmatrix}. \quad (20)$$

We apply the RTS algorithm on the real-valued system model in (19) and estimate the transmitted symbol vector. We note that the transmit and receive dimensions in the linear vector channel in (19) are $d_t = 2N_t$ and $d_r = 2N_r$.

In this section, we present the uncoded BER performance of RTS based detection of V-BLAST signals. Since the RTS algorithm is a heuristic, analytical evaluation of the BER and convergence behavior is difficult. So we evaluate the BER and convergence performance of the RTS algorithm through simulations. The following RTS parameters are used in the simulations for 4-QAM: MMSE initial vector, $P_0 = 2, \beta = 0.1, \alpha_1 = 5\%, \alpha_2 = 0.05\%, max_rep = 75, min_iter = 20$. Perfect channel state information at the receiver (CSIR) and i.i.d. fading are assumed.

A. Convergence behavior of RTS in V-BLAST

In Fig. 1, we plot the BER performance of the RTS algorithm as a function of maximum number of iterations, max_iter , in $8 \times 8, 16 \times 16, 32 \times 32$, and 64×64 V-BLAST systems with 4-QAM at an average SNR of 10 dB. Two main observations can be made from Fig. 1: *i*) for the system parameters considered, the BER converges (i.e., change in BER between successive iterations becomes very small) for max_iter greater than 300, and *ii*) the converged BER of RTS exhibits large-dimension behavior (i.e., converged BER improves with increasing $N_t = N_r$); e.g., the converged BER improves from 8.3×10^{-3} for 8×8 V-BLAST to 1.3×10^{-3} for 64×64 V-BLAST. This improvement is quite significant

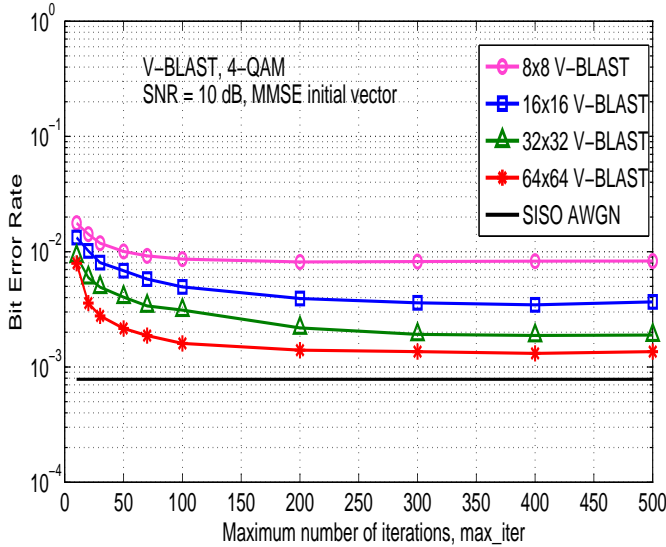


Fig. 1. Uncoded BER performance of the RTS algorithm as a function of maximum number of iterations, max_iter , in 8×8 , 16×16 , 32×32 , and 64×64 V-BLAST with 4-QAM at SNR = 10 dB.

considering that the BER in SISO AWGN channel itself is 7.8×10^{-4} for 4-QAM. We use max_iter to be 300 for 4-QAM in all the subsequent simulations in this section.

B. RTS versus LAS performance in V-BLAST

We next present the BER performance of the RTS algorithm in comparison with that of the LAS algorithm presented in [23]. Figure 2 shows the BER performance of RTS and LAS algorithms for 16×16 , 32×32 and 64×64 V-BLAST with 4-QAM. It can be seen that for the number of dimensions (i.e., N_t) considered, RTS performs better than LAS; e.g., LAS requires 128 real dimensions (i.e., 64×64 V-BLAST with 4-QAM) to achieve performance close to within 1.8 dB of SISO AWGN performance at 10^{-3} BER, whereas RTS is able to achieve even better closeness to SISO AWGN performance with just 32 real dimensions (i.e., 16×16 V-BLAST with 4-QAM). Also, in 64×64 V-BLAST, RTS achieves 10^{-3} BER at an SNR of just 0.4 dB away from SISO AWGN performance. We note that RTS is able to achieve this better performance because, while the bit/symbol-flipping strategies are similar in both RTS and LAS, the inherent escape strategy in RTS allows it to move out of local minimas and move towards better solutions. Consequently, RTS incurs some extra complexity compared to LAS as detailed in the following subsection.

C. Complexity of RTS in V-BLAST

Here, we present the complexity of the RTS algorithm for detection in V-BLAST. The total complexity comprises of three main components, namely, *i*) computation of the initial solution vector $\tilde{\mathbf{x}}^{(0)}$, *ii*) computation of $\tilde{\mathbf{H}}^T \tilde{\mathbf{H}}$, and *iii*) the reactive tabu search operation. The MMSE initial solution vector can be computed in $O(N_t^2 N_r)$ complexity, i.e., in $O(N_t N_r)$ per-symbol complexity since there are N_t symbols per channel use. Likewise, the computation of $\tilde{\mathbf{H}}^T \tilde{\mathbf{H}}$ can be done in $O(N_t N_r)$ per-symbol complexity. We note

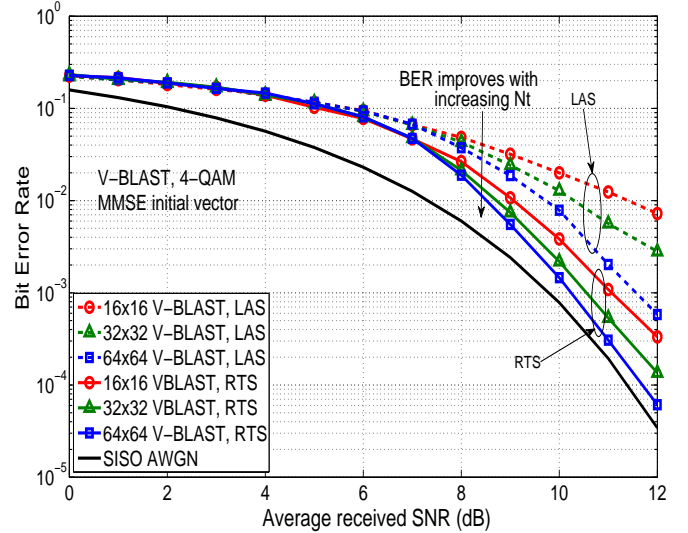


Fig. 2. Uncoded BER performance of RTS detection of 16×16 , 32×32 and 64×64 V-BLAST signals with 4-QAM.

that, since computation of $\tilde{\mathbf{x}}^{(0)}$ and $\tilde{\mathbf{H}}^T \tilde{\mathbf{H}}$ are needed in both RTS and LAS, the complexity components *i*) and *ii*) will be same for both these algorithms. We further note that, while the complexity components *i*) and *ii*) are deterministic, the component *iii*), which is due to the search part alone, is random, and so we obtained the average complexity of component *iii*) through simulations. Figure 3 shows the complexity plots for the search part alone (i.e., component *iii*) as well as the overall complexity plots of the RTS and LAS algorithms for V-BLAST with $N_t = N_r$ and 4-QAM at a BER of 10^{-2} . From Fig. 3, it can be observed that the RTS search part has a higher complexity than the LAS search part. This is expected, because the RTS can escape from a local minima and look for better solutions, whereas LAS settles in the first local minima itself. However, it can be seen that since the overall complexity is dominated by the computation of $\tilde{\mathbf{H}}^T \tilde{\mathbf{H}}$ and $\tilde{\mathbf{x}}^{(0)}$, the difference in overall complexity between RTS and LAS is not high.

D. Comparison with variants of sphere decoders in V-BLAST

In Fig. 4, we present a uncoded BER comparison of the RTS detector with the fixed-complexity sphere decoder (FSD) presented in [12] for V-BLAST with $N_t = N_r = 4, 8, 16, 32$ and 4-QAM. The performance of the reduced-complexity sphere decoder (RSD) presented in [13] is also plotted for $N_t = N_r = 4, 8, 16$. We did not evaluate the performance of RSD for $N_t = N_r = 32$ due to its high complexity. Comparing the performances of FSD, RSD and RTS in Fig. 4, we observe the following:

- 1) Since the complexity of FSD is forced to be constant, the performance of FSD is compromised at low/medium SNRs compared to that of RSD (e.g., see plots for $N_t = N_r = 16$, where RSD performs better than FSD by about 1 dB at 10^{-2} BER).
- 2) Performance of RTS is very close to that of RSD (see plots of RSD and RTS for $N_t = N_r = 16$). RTS

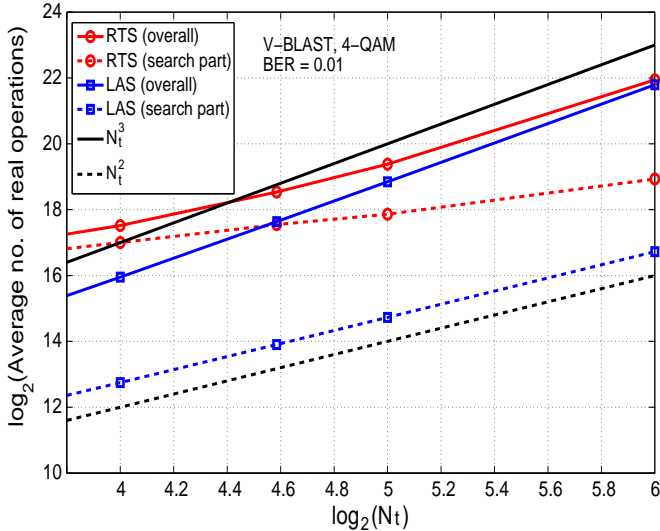


Fig. 3. Complexity comparison of RTS and LAS algorithms in detection of V-BLAST signals with 4-QAM at 10^{-2} BER.

achieves such good performance in large dimensions at a significantly lesser complexity compared to that of RSD (see complexity comparison in Table 1 for 16×16 V-BLAST).

- For large number of antennas (e.g., $N_t = N_r = 32$), RSD complexity becomes prohibitively high, and so we do not show its performance for 32×32 V-BLAST. However, we have shown the FSD and RTS performances for 32×32 V-BLAST. It is seen that RTS performs significantly better than FSD (by about 1.5 dB at 10^{-2} BER); this is due to the sub-optimum nature of FSD that arises because of fixing its complexity, and due to the large-dimension behavior advantage of RTS. In addition, RTS achieves this better performance than FSD at a significantly lesser complexity compared to that of FSD (see details in the complexity comparison text in the following paragraphs and the 32×32 system entries in Table 1).

Complexity comparison between RTS and FSD in V-BLAST: The FSD algorithm in [12] has two parts; an ordering part (similar to that in V-BLAST algorithm) and a search part. The complexity of the search part, which is random in conventional SD, is made constant in FSD by fixing the number of search candidates irrespective of the SNR. The ordering part has $O(N_t^3)$ complexity in N_t . Also, the algorithm has $O(M^{\lceil \sqrt{N_t}-1 \rceil})$ complexity in M (i.e., alphabet size) for $N_t = N_r$ [12]. On the other hand, while RTS also has $O(N_t^3)$ complexity in N_t in a V-BLAST system, its complexity in M is just $O(MN_t)$ since at most $(M-1)N_t$ neighbors need to be considered. The exponential complexity of FSD in $\sqrt{N_t}$ makes it increasingly prohibitive for increasing N_t . For e.g., for $N_t = N_r = 32$ and 16-QAM, the complexity of FSD, which is dominated by $O(M^{\lceil \sqrt{N_t}-1 \rceil})$, is $O(16^5) = O(2^{20})$. For the same system settings, the RTS complexity is dominated by $O(N_t^3)$, which is $O(32^3) = O(2^{15})$. The differential in complexity between RTS and FSD (in favor of RTS) widens

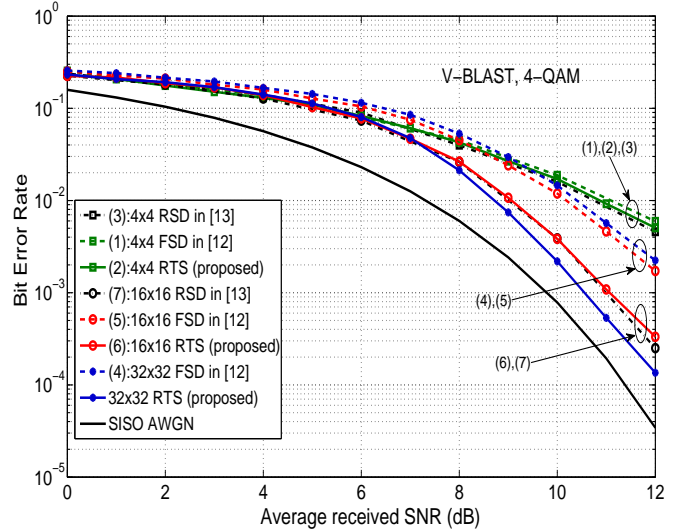


Fig. 4. Comparison of uncoded BER performance of V-BLAST using RTS detection versus fixed-complexity sphere decoding in [12] and reduced complexity sphere decoder in [13] for $N_t = N_r = 4, 8, 16, 32$ and 4-QAM. RSD performance for 32×32 V-BLAST is not shown due to its high complexity.

further if 64-QAM is considered.

A complexity comparison along with performance comparison between different detectors is shown in Table 1, where we have presented the per-symbol complexity (measured in number of real operations) and the SNR required to achieve an uncoded BER of 10^{-2} in 4×4 , 8×8 , 16×16 and 32×32 V-BLAST systems with 4-QAM. From Table 1, we see that the complexity of FSD for 32×32 V-BLAST is about an order higher compared to that of RTS, due to the $O(M^{\lceil \sqrt{N_t}-1 \rceil})$ complexity of FSD. Also, even with this higher complexity, FSD achieves poorer performance than RTS (i.e., FSD needs about 1.5 dB more SNR than required by RTS to achieve 10^{-2} BER), as described earlier.

E. Higher-Order QAM Performance in V-BLAST

In Fig. 5, we illustrate the performance of RTS for higher-order QAM in a 32×32 V-BLAST system (16-QAM and 64-QAM at spectral efficiencies of 128 bps/Hz and 192 bps/Hz). We do not give the performance of FSD and RSD due to their high complexities for the considered values of N_t and M . As we mentioned earlier, FSD complexity for $N_t = N_r = 32$ and $M = 64$ would be $O(64^{\lceil \sqrt{32}-1 \rceil}) = O(2^{30})$, which is prohibitive. The complexities of RTS and LAS, on the other hand, scale well for such large dimensions, allowing us to show their simulated BER performance in Fig. 5. The following RTS parameters are used in the simulations: MMSE initial vector, $P_0 = 2$, $\beta = 0.01$; ($N = 3$, $\alpha_1 = 0.3\%$, $\alpha_2 = 0.001\%$, $max_rep = 250$, $min_iter = 30$, $max_iter = 1000$) for 16-QAM, and ($N = 2$, $\alpha_1 = 0.005\%$, $\alpha_2 = 0.00005\%$, $max_rep = 1000$, $min_iter = 50$, $max_iter = 3000$) for 64-QAM. The plots in Fig. 5 show that RTS performs better than LAS by about 6 dB at 10^{-2} BER for 16-QAM and 64-QAM.

Detector Algorithm	Per-symbol-complexity (PSC) in number of real operations and SNR required to achieve 10^{-2} uncoded BER for 4-QAM (Ref: Fig. 4)								Order of total complexity in M and N_t
	4×4		8×8		16×16		32×32		
	PSC	SNR	PSC	SNR	PSC	SNR	PSC	SNR	
RTS (proposed)	5,540	10.9 dB	9,469	9.7 dB	11,730	9 dB	21,320	8.8 dB	$O(MN_t) + O(N_t^3)$
FSD in [12]	355	11 dB	1,621	10.1 dB	8,445	10.1 dB	155,253	10.3 dB	$O(M^{\lceil \sqrt{N_t} - 1 \rceil}) + O(N_t^3)$
RSD in [13]	662	10.8 dB	2,881	9.7 dB	64,217	9 dB	-	-	-

TABLE I

COMPLEXITY AND PERFORMANCE COMPARISON OF THE RTS ALGORITHM WITH THE FSD ALGORITHM IN [12] AND THE RSD ALGORITHM IN [13] IN 4×4 , 8×8 , 16×16 AND 32×32 V-BLAST WITH 4-QAM. RTS OUTPERFORMS FSD IN TERMS OF COMPLEXITY AND PERFORMANCE FOR LARGE DIMENSIONS (E.G., 32×32). FOR LARGE M AND LARGE N_t , COMPLEXITY OF FSD GETS PROHIBITIVELY HIGH.

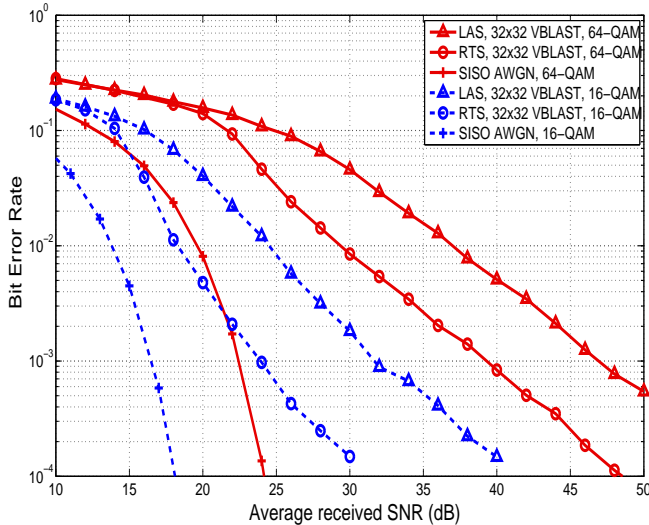


Fig. 5. Uncoded BER performance of RTS and LAS algorithms for 32×32 V-BLAST system with 16-QAM and 64-QAM. FSD and RSD performances are not shown due to their high complexities.

IV. RTS PERFORMANCE IN LARGE NON-ORTHOGONAL STBCs

Large-MIMO systems that employ non-orthogonal STBCs from CDA [14],[15] are attractive because these STBCs can simultaneously provide both *full rate* (i.e., N_t complex symbols per channel use, which is the same as in V-BLAST) as well as *full transmit diversity* (V-BLAST does not provide transmit diversity). The 2×2 Golden code is a well known non-orthogonal STBC from CDA for 2 transmit antennas [16]. A non-orthogonal STBC from CDA is a $N_t \times N_t$ matrix whose entries are formed using linear combinations of various data symbols [14]. Each STBC matrix is constructed using N_t^2 data symbols, which are sent in using N_t transmit antennas in N_t channel uses. The received signal matrix can be vectorized and written in an equivalent real system model of the form (19), where the number of transmit and receive dimensions are $d_t = 2N_t^2$ and $d_r = 2N_t N_r$, respectively, for QAM [23].

High spectral efficiencies can be achieved using *large* non-orthogonal STBCs from CDA. For e.g., a 16×16 STBC from CDA has 256 complex symbols in it with 512 *real dimensions*; with 16-QAM and rate-3/4 turbo code, this system offers a high spectral efficiency of 48 bps/Hz. Variants of sphere decoding (e.g., FSD [12] and RSD [13]) do not scale well to decode signals with hundreds of dimensions². In [23], we have shown that the LAS algorithm can scale well to such hundreds of dimensions while achieving good performance. In this section, we show that RTS also scales well in complexity in decoding large non-orthogonal STBCs from CDA having hundreds of dimensions, while achieving even better performance than LAS.

RTS complexity in decoding non-orthogonal STBCs from CDA: Here again, $\tilde{\mathbf{H}}^T \tilde{\mathbf{H}}$ computation complexity dominates the overall complexity compared to the search complexity. Note that there $2N_t^2$ transmit and $2N_t N_r$ receive dimensions, and N_t^2 symbols per STBC. Exploiting the permutation nature of the weight matrices of the non-orthogonal STBCs from CDA [23], the per-symbol complexity of computing $\tilde{\mathbf{H}}^T \tilde{\mathbf{H}}$, and hence the overall per-symbol complexity in RTS decoding of non-orthogonal STBCs from CDA is $O(N_t^2 N_r)$.

In the following subsections, we present the BER performance of RTS in decoding non-orthogonal STBCs. The following parameters are used in the simulations for 4-QAM: MMSE initial vector, $P_0 = 2, \beta = 1, \alpha_1 = 5\%, \alpha_2 = 0.05\%, \max_rep = 75, \min_iter = 20, \max_iter = 300$.

A. RTS versus LAS performance in decoding non-orthogonal STBCs

In Fig. 6, we plot the uncoded BER of the RTS algorithm as a function of average received SNR in decoding 4×4 (32 dimensions), 8×8 (128 dimensions) and 12×12 (288 dimensions) non-orthogonal STBCs from CDA for 4-QAM and $N_t = N_r$. Perfect CSIR and i.i.d fading are assumed. For the same settings, performance of the LAS algorithm is

²Since FSD and RSD complexities are prohibitive to decode signals with hundreds of dimensions, we do not present the performance of FSD and RSD for large non-orthogonal STBCs.

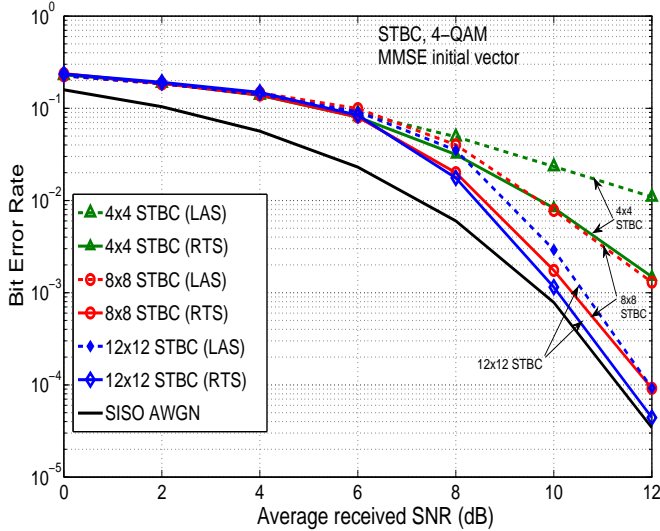


Fig. 6. Uncoded BER of RTS decoding of 4×4 , 8×8 , and 12×12 non-orthogonal STBCs from CDA for $N_t = N_r$ and 4-QAM.

also plotted for comparison. MMSE initial vector is used in both RTS and LAS. As a lower bound on performance, we have plotted the BER performance on a SISO AWGN channel as well. From Fig. 6, it can be observed that the BER of RTS improves and approaches SISO AWGN performance as $N_t = N_r$ (i.e., STBC size) is increased; e.g., with 12×12 STBC having 288 dimensions, RTS decoding is able to achieve close to within 0.4 dB from SISO AWGN performance at 10^{-3} uncoded BER. Also, as in the case of V-BLAST, RTS is found to perform better than LAS in decoding non-orthogonal STBCs as well. In the case of 16-QAM also, RTS performs better than LAS as can be seen in Fig. ??, where the following parameters are used in the simulations: MMSE initial vector, $P_0 = 2, \beta = 1, N = 3, \alpha_1 = 0.1\%, \alpha_2 = 0.002\%, \max_rep = 75, \min_iter = 30, \max_iter = 800$.

B. Turbo coded BER performance of RTS

Figure 7 shows the rate-3/4 turbo coded BER performance of RTS decoding of 12×12 non-orthogonal STBC from CDA with $N_t = N_r$ and 4-QAM (corresponding to a spectral efficiency of 18 bps/Hz), under perfect CSIR and i.i.d fading. The theoretical minimum SNR required to achieve 18 bps/Hz spectral efficiency on a $N_t = N_r = 12$ MIMO channel with perfect CSIR and i.i.d fading is 4.27 dB (obtained through simulation of the ergodic MIMO capacity formula [24]). From Fig. 7, it is seen that RTS decoding is able to achieve vertical fall in coded BER close to within about 5 dB from the theoretical minimum SNR, which is a good nearness to capacity performance. This nearness to capacity can be further improved by 1 to 1.5 dB if soft decision values, proposed in [23], are fed to the turbo decoder. Also, the performance of RTS is about 1 dB better than that of LAS at 2×10^{-4} coded BER for the same system settings.

C. Iterative RTS Decoding/Channel Estimation

Next, we relax the perfect CSIR assumption by considering a training based iterative RTS decoding/channel estimation

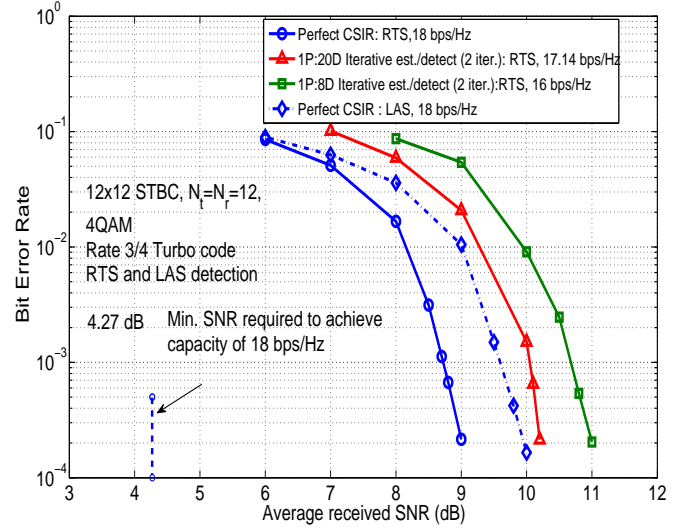


Fig. 7. Turbo coded BER of RTS decoding of 12×12 non-orthogonal STBC from CDA with $N_t = N_r$, 4-QAM, rate-3/4 turbo code, and 18 bps/Hz with perfect CSIR and estimated CSIR.

scheme. Transmission is carried out in frames, where one $N_t \times N_t$ pilot matrix (for training purposes) followed by N_d data STBC matrices are sent in each frame [23]. One frame length, T , (taken to be the channel coherence time) is $T = (N_d + 1)N_t$ channel uses. The proposed scheme works as follows: *i*) obtain an MMSE estimate of the channel matrix during the pilot phase, *ii*) use the estimated channel matrix to decode the data STBC matrices using RTS, *iii*) use the decoded STBCs to estimate the channel matrix again, and *iv*) iterate between channel estimation and RTS decoding for a certain number of times. For 12×12 STBC from CDA, in addition to perfect CSIR performance, Fig. 7 also shows the performance with CSIR estimated using the above iterative RTS decoding/channel estimation scheme for $N_d = 8$ and $N_d = 20$. 2 iterations between RTS decoding and channel estimation are used. With $N_d = 20$ (which corresponds to large coherence times, i.e., slow fading) the BER and bps/Hz with estimated CSIR get closer to those with perfect CSIR.

D. Effect of MIMO Spatial Correlation

In all the previous performance and complexity plots, we assumed i.i.d fading. But spatial correlation at transmit/receive antennas and the structure of scattering and propagation environment can affect the rank structure of the MIMO channel resulting in degraded performance [25],[26]. We relaxed the i.i.d. fading assumption by considering the correlated MIMO channel model proposed by Gesbert *et al* in [26], which takes into account carrier frequency (f_c), spacing between antenna elements (l_t, l_r), distance between transmit and receive antennas (D), and scattering environment. In Fig. 8, we plot the uncoded BER of RTS decoding of 12×12 STBC from CDA with perfect CSIR in *i*) i.i.d. fading, and *ii*) correlated MIMO fading model in [26]. It is seen that, compared to i.i.d fading, there is a performance loss in spatial correlation for $N_t = N_r = 12$; further, use of more receive antennas ($N_r = 14, N_t = 12$) alleviates this loss in performance.

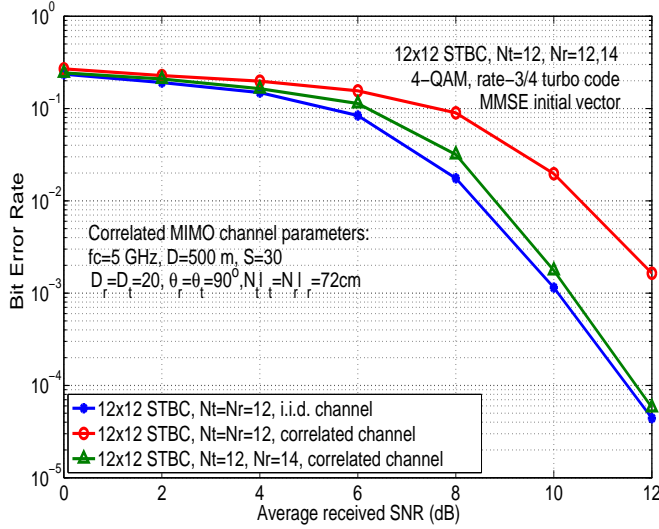


Fig. 8. Effect of spatial correlation on the performance of RTS decoding of 12×12 STBC from CDA with $N_t = 12$, $N_r = 12, 14$, 4-QAM, rate-3/4 turbo code, 18 bps/Hz. $f_c = 5$ GHz, $D = 500$ m, $S = 30$, $D_t = D_r = 20$ m, $\theta_t = \theta_r = 90^\circ$, $N_r l_r = N_t l_t = 72$ cm.

V. RTS EQUALIZER FOR MIMO-ISI CHANNELS

In this section, we consider the adoption and performance of the RTS algorithm in another communication scheme, where large dimensions are created in time due to the highly frequency selective nature of the channel, i.e., large number (tens to hundreds) of multipath components (MPC), as can typically happen in UWB channels [17],[20].

Consider a frequency-selective MIMO channel with N_t transmit and N_r receive antennas (Fig. 9). Let L denote the number of MPCs. Data is transmitted in frames, where each frame has K data symbols preceded by a cyclic prefix (CP) of length L symbols, $K \geq L$. While CP avoids inter-frame interference, there will be ISI within the frame. Let $\mathbf{x}_q \in \mathbb{A}^{N_t}$ be the transmitted symbol at time q , $0 \leq q \leq K-1$, where \mathbb{A} is the transmit symbol alphabet, which is taken to be M -QAM. The received signal vector at time q can be written as

$$\mathbf{y}_q = \sum_{l=0}^{L-1} \mathbf{H}_l \mathbf{x}_{q-l} + \mathbf{w}_q, \quad q = 0, \dots, K-1, \quad (21)$$

where $\mathbf{y}_q \in \mathbb{C}^{N_r \times 1}$, $\mathbf{H}_l \in \mathbb{C}^{N_r \times N_t}$ is the channel gain matrix for the l th MPC. The entries of \mathbf{H}_l are assumed to be random with distribution $\mathcal{CN}(0, 1)$. It is further assumed that \mathbf{H}_l , $l = 0, \dots, L-1$ do not change for one frame duration. $\mathbf{w}_q \in \mathbb{C}^{N_r \times 1}$ is the additive white Gaussian noise vector at time q , whose entries are independent, each with variance N_0 . The CP will render the linearly convolving channel to a circularly convolving one, and so the channel will be multiplicative in frequency domain. Because of the CP, the received signal in frequency domain, for the i th frequency index ($0 \leq i \leq K-1$), can be written as

$$\mathbf{r}_i = \mathbf{G}_i \mathbf{u}_i + \mathbf{v}_i, \quad (22)$$

$$\text{where } \mathbf{r}_i = \frac{1}{\sqrt{K}} \sum_{q=0}^{K-1} e^{-\frac{2\pi j q i}{K}} \mathbf{y}_q, \quad \mathbf{j} = \sqrt{-1}, \quad \mathbf{u}_i =$$

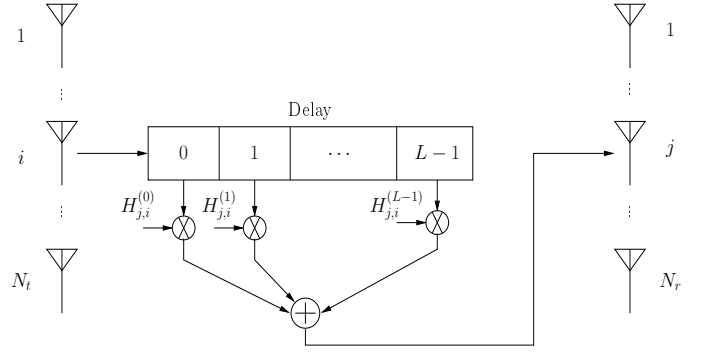


Fig. 9. MIMO-ISI channel model.

$\frac{1}{\sqrt{K}} \sum_{q=0}^{K-1} e^{-\frac{2\pi j q i}{K}} \mathbf{x}_q$, $\mathbf{v}_i = \frac{1}{\sqrt{K}} \sum_{q=0}^{K-1} e^{-\frac{2\pi j q i}{K}} \mathbf{w}_q$, and $\mathbf{G}_i = \sum_{l=0}^{L-1} e^{-\frac{2\pi j l i}{K}} \mathbf{H}_l$. Stacking the K vectors \mathbf{r}_i , $i = 0, \dots, K-1$, we can write

$$\mathbf{r} = \underbrace{\mathbf{G}}_{\triangleq \mathbf{H}_{eff}} \mathbf{x}_{eff} + \mathbf{v}_{eff}, \quad (23)$$

where

$$\mathbf{r} = \begin{bmatrix} \mathbf{r}_0 \\ \mathbf{r}_1 \\ \vdots \\ \mathbf{r}_{K-1} \end{bmatrix}, \quad \mathbf{G} = \begin{bmatrix} \mathbf{G}_0 & & & \mathbf{0} \\ & \mathbf{G}_1 & & \\ & & \ddots & \\ \mathbf{0} & & & \mathbf{G}_{K-1} \end{bmatrix},$$

$$\mathbf{x}_{eff} = \begin{bmatrix} \mathbf{x}_0 \\ \mathbf{x}_1 \\ \vdots \\ \mathbf{x}_{K-1} \end{bmatrix}, \quad \mathbf{v}_{eff} = \begin{bmatrix} \mathbf{v}_0 \\ \mathbf{v}_1 \\ \vdots \\ \mathbf{v}_{K-1} \end{bmatrix},$$

$$\mathbf{F} = \frac{1}{\sqrt{K}} \begin{bmatrix} \rho_{0,0} \mathbf{I}_{N_t} & \rho_{1,0} \mathbf{I}_{N_t} & \cdots & \rho_{K-1,0} \mathbf{I}_{N_t} \\ \rho_{0,1} \mathbf{I}_{N_t} & \rho_{1,1} \mathbf{I}_{N_t} & \cdots & \rho_{K-1,1} \mathbf{I}_{N_t} \\ \vdots & \vdots & \cdots & \vdots \\ \rho_{0,K-1} \mathbf{I}_{N_t} & \rho_{1,K-1} \mathbf{I}_{N_t} & \cdots & \rho_{K-1,K-1} \mathbf{I}_{N_t} \end{bmatrix} \\ = \frac{1}{\sqrt{K}} \mathbf{D}_K \otimes \mathbf{I}_{N_t},$$

where $\rho_{q,i} = e^{-\frac{2\pi j q i}{K}}$, \mathbf{D}_K is the K -point DFT matrix and \otimes denotes the Kronecker product. The received signal model in (23) can be rewritten in real form with $d_t = 2N_t K$ and $d_r = 2N_r K$. RTS algorithm is applied on this real-valued system model.

Initial vector using FD-MMSE equalizer: The detected symbol vector obtained using frequency domain (FD) MMSE equalization can be used as the initial vector to the RTS algorithm. The FD-MMSE equalizer on the i th frequency employs MMSE nulling as

$$\hat{\mathbf{u}}_i = \left(\mathbf{G}_i^H \mathbf{G}_i + \frac{N_0}{E_s} \mathbf{I}_{N_t} \right)^{-1} \mathbf{G}_i^H \mathbf{r}_i, \quad 0 \leq i \leq K-1 \quad (24)$$

where E_s is the average energy of a transmitted symbol. The $\hat{\mathbf{u}}_i$'s are transformed back to time domain using K -point IDFT

to obtain an estimate of the transmitted symbol vector as

$$\hat{\mathbf{x}}_q = \frac{1}{\sqrt{K}} \sum_{i=0}^{K-1} e^{\frac{2\pi i q i}{K}} \hat{\mathbf{u}}_i, \quad 0 \leq q \leq K-1, \quad (25)$$

which are used to form the initial vector to the RTS algorithm

A. Performance Results and Discussions

We evaluated the BER performance of the proposed RTS equalizer in a 4×4 MIMO V-BLAST system with 4-QAM as a function of average E_b/N_0 per receive antenna, through simulations. We have assumed uniform power delay profile (i.e., all the L paths are assumed to be of equal energy) We evaluated the performance for various number of delay paths, L , and frame sizes, K , keeping L/K constant. It is noted that the system becomes a ‘large-dimension system’ when L and K are increased keeping L/K fixed. The FD-MMSE equalizer output is used as the initial vector for both RTS and LAS. The following RTS parameters are used: $P_0 = 2$; $\beta = 1$; $\alpha_1 = 0.03$; $max_rep = 75$; $min_iter = 30$. For $K = 64$ and 128 , $max_iter = 300$ and $\alpha_2 = 0.00075$. For $K = 512$, $max_iter = 500$ and $\alpha_2 = 0.0004$.

In Fig. 10, we plot the uncoded BER of the RTS equalizer for $(L = 6, K = 64)$, $(L = 12, K = 128)$, and $(L = 48, K = 512)$, $L/K = 0.09375$. Note that for $(L = 48, K = 512)$, the number of transmit dimensions is $d_t = 2N_t K = 2 \times 4 \times 512 = 4096$ dimensions. Since FSD and RSD complexities are prohibitive for number of dimensions in the thousands, we do not give their performances. In addition to the performance of RTS, we have given the performance of *i*) the FD-MMSE equalizer (without any subsequent search), *ii*) LAS equalizer, and *iii*) single-input multiple-output (SIMO) AWGN with $N_r = 4$ (which can be viewed as a good lower bound on the best detector performance). It is seen that the performance of the FD-MMSE equalizer is poor. However, the subsequent search operations carried out in RTS and LAS result in significantly improved performance for increasing L, K . Both RTS and LAS show large-dimension behavior in this system also (i.e., BER improves for increasing L, K , keeping L/K fixed). For a given L , RTS performs better than LAS. For e.g., at 10^{-3} BER, RTS performs better by about 1.5 dB and 0.8 dB compared LAS for $(L = 6, K = 64)$ and $(L = 12, K = 128)$, respectively. We note that the per-symbol complexity of FD-MMSE (i.e., initial vector) computation is $O(KN_t + N_t^2)$. The per-symbol complexity of $\tilde{\mathbf{H}}^T \tilde{\mathbf{H}}$ computation is $O(K^2 N_t)$. The per-symbol search complexities for RTS, obtained by simulations, is $O(KN_t)$. So the overall per-symbol complexity of the RTS equalizer is $O(K^2 N_t) + O(KN_t + N_t^2)$.

VI. CONCLUSIONS

We conclude by highlighting some recent trends in high spectral efficiency MIMO systems/measurements with large number of antennas to bring out the contextual importance and relevance of the work presented in this paper. 1) NTT DoCoMo has already field demonstrated a 12×12 V-BLAST system operating at 5 Gbps data rate and 50 bps/Hz spectral efficiency in 4.6 GHz band at a mobile speed of 10 Km/hr [29].

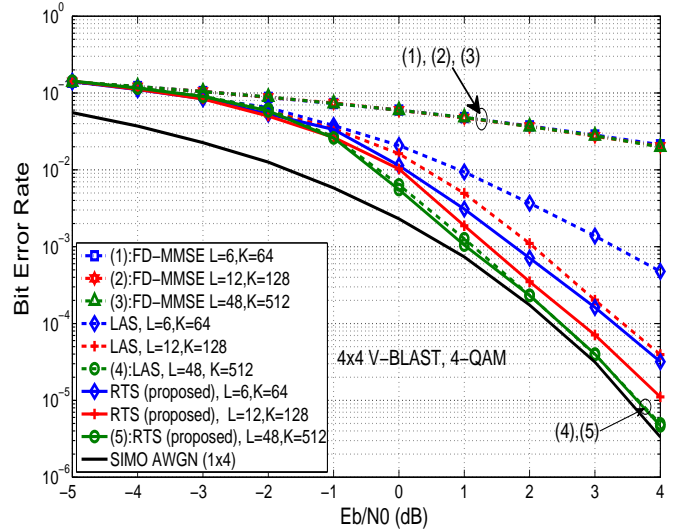


Fig. 10. Comparison of the BER performance of the proposed RTS equalizer with those of LAS equalizer and FD-MMSE equalizer in a 4×4 V-BLAST system with 4-QAM for different number of MPCs (L) and frame sizes (K), keeping L/K constant. Uniform power delay profile.

2) Evolution of WiFi standards (evolution from IEEE 802.11n to IEEE 802.11ac to achieve multi-gigabit rate transmissions in 5 GHz band) now considers 16×16 MIMO operation; e.g., see 16×16 MIMO indoor channel sounding measurements at 5.17 GHz reported in [30] for consideration in WiFi standards. 3) 64×64 MIMO channel sounding measurements at 5 GHz in indoor environments have been reported in [31]. We note that, while the RF/antenna technologies/measurements for large-MIMO systems are getting matured, there is lack of current focus on development of low-complexity baseband algorithms for detection and channel estimation for large-MIMO systems (MIMO systems with 16 or more antennas) to reap their high spectral efficiency benefits. A vast body of MIMO detection literature is heavily focused on 4×4 (in some cases 8×8) MIMO. Algorithms suited for large-MIMO signal detection and their performance have started appearing in the literature recently (e.g., [22],[23]). Here, we showed that the RTS algorithm presented in this paper achieves even better performance than the LAS algorithm presented in [23] (e.g., 6 dB better performance in 32×32 V-BLAST with 16- and 64-QAM in Fig. 5). We also showed that the considered sphere decoding variants (FSD, RSD) either performed poorly and/or did not scale well for large-dimension detection (e.g., see 32×32 V-BLAST plots and complexities in Fig. 4 and Table 1). The large-dimension behavior of the RTS algorithm has other potential applications, like the low-complexity equalization in severely delay-spread UWB systems (with thousands of dimensions) presented in this paper. Finally, we note that algorithms for low-complexity, high-performance large-dimension signal processing for communication applications is a promising research direction.

REFERENCES

- [1] I. E. Telatar, ‘‘Capacity of multi-antenna Gaussian channels,’’ *European Trans. Telecommun.*, vol. 10, no. 6, pp. 585-595, November 1999.

- [2] A. Paulraj, R. Nabar, and D. Gore, *Introduction to Space-Time Wireless Communications*, Cambridge University Press, 2003.
- [3] X. Shen, M. Guizani, R. C. Qiu, and T. Le-Ngoc, *Ultrawideband Wireless Communications and Networks*, John Wiley & Sons, 2006.
- [4] V. J. Rayward-Smith, I. H. Osman, C. R. Reeves, and G. D. Smith, Editors, *Modern Heuristic Search Methods*, John Wiley & Sons, 1996.
- [5] F. Glover, "Tabu Search - Part I," *ORSA Jl. of Computing*, vol. 1, no. 3, Summer 1989, pp. 190-206.
- [6] F. Glover, "Tabu Search - Part II," *ORSA Jl. of Computing*, vol. 2, no. 1, Winter 1990, pp. 4-32.
- [7] F. Glover and M. Laguna, "Tabu Search - Modern Heuristic Techniques for Combinatorial Problems," Colin R. Reeves Ed., 70-150, Blackwell Scientific Publications, Oxford, 1993.
- [8] R. Battiti, G. Tecchiolli, "The reactive tabu search," *ORSA Jl. on Computing*, no. 2, pp. 126-140, 1994.
- [9] Y. Huang and J. A. Ritcey, "Improved 16-QAM constellation labeling for BI-STCM-ID with the Alamouti scheme," *IEEE Commun. Letters*, vol. 9, no. 2, pp. 157-159, February 2005.
- [10] P. H. Tan and L. K. Rasmussen, "Multiuser detection in CDMA - A comparison of relaxations, exact, and heuristic search methods," *IEEE Trans. Wireless Commun.*, vol. 3, no. 5, pp. 1802-1809, September 2004.
- [11] H. Zhao, H. Long, W. Wang, "Tabu search detection for MIMO systems," *PIMRC'2007*, Athens, September 2007.
- [12] L. G. Barbero and J. S. Thompson, "Fixing the complexity of the sphere decoder for MIMO detection," *IEEE Trans. Wireless Commun.*, vol. 7, no. 6, pp. 2131-2142, June 2008.
- [13] Y. Wang and K. Roy, "A new reduced complexity sphere decoder with true lattice boundary awareness for multi-antenna systems," *IEEE ISCAS'2005*, vol. 5, pp. 4963-4966, May 2005.
- [14] B. A. Sethuraman, B. Sundar Rajan, V. Shashidhar, "Full-diversity high-rate space-time block codes from division algebras," *IEEE Trans. Inform. Theory*, vol. 49, no. 10, pp. 2596-2616, October 2003.
- [15] F. Oggier, J.-C. Belfiore, and E. Viterbo, *Cyclic Division Algebras: A Tool for Space-Time Coding*, Foundations and Trends in Commun. and Inform. Theory, vol. 4, no. 1, pp. 1-95, Now Publishers, 2007.
- [16] J.-C. Belfiore, G. Rekaya, and E. Viterbo, "The golden code: A 2×2 full-rate space-time code with non-vanishing determinants," *IEEE Trans. Inform. Theory*, vol. 51, no. 4, April 2005.
- [17] A. F. Molisch, J. R. Foerster, M. Pendergrass, "Channel models for ultrawideband personal area networks," *IEEE Wireless Commun.*, vol. 10, no. 6, pp. 1421, December 2003.
- [18] A. F. Molisch, "Ultrawideband propagation channels - Theory, measurement, and modeling," *IEEE Trans. Veh. Tech.*, vol. 54, no. 5, pp. 1528-1545, September 2005.
- [19] J. Karedal, S. Wyne, P. Almers, F. Tufvesson, and A. F. Molisch, "Statistical analysis of the UWB channel in an industrial environment," *Proc. IEEE VTC'2004-Fall*, pp. 81-85, September 2004.
- [20] R. Saadane and A. Menouni Hayar, "DRB1.3 third report on UWB channel models," NewCom, <http://www.eurecom.fr/util/publidownload.fr.htm?id=2112>, Nov. 2006.
- [21] Y. Sun, "A family of linear complexity likelihood ascent search detectors for CDMA multiuser detection," *Proc. IEEE 6th Intl. Symp. on Spread Spectrum Tech. & App.*, September 2000.
- [22] K. Vishnu Vardhan, Saif K. Mohammed, A. Chockalingam, and B. Sundar Rajan, "A low-complexity detector for large MIMO systems and multicarrier CDMA systems," *IEEE JSAC Spl. Iss. on Multiuser Detection for Adv. Commun. Systems and Networks*, vol. 26, no. 3, pp. 473-485, April 2008.
- [23] Saif K. Mohammed, Ahmed Zaki, A. Chockalingam, and B. Sundar Rajan, "High-rate space-time coded large-MIMO systems: Low-complexity detection and channel estimation," to appear in *IEEE Jl. Sel. Topics in Signal Processing (JSTSP): Spl. Iss. on Managing Complexity in Multiuser MIMO Systems*, December 2009. Online arXiv:0809.2446v3 [cs.IT] 16 Sept 2009.
- [24] H. Jafarkhani, *Space-Time Coding: Theory and Practice*, Cambridge University Press, 2005.
- [25] D. Shiu, G. J. Foschini, M. J. Gans, and J. M. Khan, "Fading correlation and its effect on the capacity of multi-antenna systems," *IEEE Trans. on Commun.*, vol. 48, pp. 502-513, March 2000.
- [26] D. Gesbert, H. Bölcskei, D. A. Gore, and A. J. Paulraj, "Outdoor MIMO wireless channels: Models and performance prediction," *IEEE Trans. on Commun.*, vol. 50, pp. 1926-1934, December 2002.
- [27] T. Wo and P. A. Hoeher, "A simple iterative Gaussian detector for severely delay-spread MIMO channels," *Proc. IEEE ICC'2007*, June 2007.
- [28] T. Koike, "Bit-flipping equalizer and ML search space analysis in ultra-wideband MIMO channels," *Proc. IEEE GLOBECOM'2008*, November-December 2008.
- [29] H. Taoka and K. Higuchi, "Field experiment on 5-Gbit/s ultra-high-speed packet transmission using MIMO multiplexing in broadband packet radio access," *NTT DoCoMo Tech. Journ.*, vol. 9, no. 2, pp. 25-31, September 2007.
- [30] Gregory Breit et al, *802.11ac Channel Modeling*, doc. IEEE 802.11-09/0088r0, submission to Task Group TGac, 19 January 2009.
- [31] J. Koivunen, *Characterisation of MIMO Propagation Channel in Multi-link Scenarios*, MS Thesis, Helsinki University of Technology, December 2007.